Rashba interferometers: Spin-dependent single and two-electron interference

U. Zülicke [a,b,*], A. I. Signal [a]

[a]*Institute of Fundamental Sciences, Massey University, Private Bag 11 222, Palmerston North, New Zealand*
[b]*MacDiarmid Institute for Advanced Materials and Nanotechnology, Massey University, Private Bag 11 222, Palmerston North, New Zealand*

Abstract

Quantum transport in semiconductor nanostructures can be described theoretically in terms of the propagation and scattering of electron probability waves. Within this approach, elements of a phase-coherent electric circuit play a role similar to quantum-optical devices that can be characterised by scattering matrices. Electronic analogues of well-know optical interferometers have been fabricated and used to study special features of charge carriers in solids. We present results from our theoretical investigation into the interplay between spin precession and quantum interference in an electronic Mach-Zehnder interferometer with spin-orbit coupling of the Rashba type. Intriguing spin-dependent transport effects occur, which can be the basis for novel spintronic devices such as a magnet-less spin-controlled field-effect transistor and a variety of single-qubit gates. Their functionality arises entirely from spin-dependent interference of each single input electron with itself. We have also studied two-electron interference effects for the spin-dependent Mach-Zehnder interferometer, obtaining analytical expressions for its two-fermion-state scattering matrix. Using this result, we consider ways to generate two-electron output states for which the Rashba spin-subband quantum number and the output-arm index are entangled. Combining spin-dependent interference in our proposed Mach-Zehnder interferometer with a projective charge measurement at the output enables entanglement generation. As our particular scheme involves tuneable spin precession, electric-field control of entanglement production can be achieved.

Key words: Phase-coherent electron transport, spintronics, electronic Mach-Zehnder interferometer, entanglement extraction
PACS: 73.43.Cd, 73.43.Jn

1. Introduction

The quantum superposition principle governing the microscopic world can be most clearly demonstrated by interference effects involving quantum particles. A famous [1] example is Feynman's double-slit *Gedankenexperiment* with electrons, which was later realised [2] using an electron-microscopy setup. While quantum interference and phase coherence have long been a central issue in quantum optics [3], mesoscopic electron transport [4] has only comparatively recently provided a versatile testing ground for these concepts in a solid-state context. Quantum phase coherence of electrons in conductors results in well-studied bulk effects such as weak localisation and universal conductance fluctuations [5]. However, the advent of micro- and nanofabrication techniques has lifted the study of phase-coherent electron transport onto a new level. It has made it possible, e.g., to observe Aharonov-Bohm [6] oscillations of

the electrical conductance through mesoscopic rings [7,8] and enabled the design of the first solid-state electron interferometers [9–11]. By now, electronic versions [12–16] of optical interferometers have been fabricated and studied in great detail. Interference of electron waves scattered by impurities or gates in a semiconductor heterostructure was imaged using scanning-probe microscopy [17,18]. In addition to providing us with a better fundamental understanding of quantum effects in solids, the study of phase-coherent transport can also lead to the design of novel electronic devices [19]. In particular, linear-optics-inspired architectures [20] for quantum information processing may eventually enable the creation of solid-state flying qubits [21].

The expectation that greater functionality of electronic devices can be achieved by utilising a charge carrier's spin degree of freedom is generating a lot of interest in studying spin-dependent transport effects [22–24]. Spin dependence can simply be introduced by the presence of magnetic materials. Based in this concept, a spin-dependent electronic Fabry-Pérot interferometer was realised in a magnetic multilayer [25,26]. More recently, state-of-the-art semiconductor engineering has made it possible to investigate the

---

* Corresponding author. *Tel.:* +64 6 350 5799 extn 7259, *fax:* +64 6 350 5682.
   Email address: u.zuelicke@massey.ac.nz (U. Zülicke).

interplay between phase coherence and spin dependence of electronic transport in *nonmagnetic* nanostructures [27–30]. Theoretical proposals for spin-dependent electronic Aharonov-Bohm [31–38], Sagnac [39], Mach-Zehnder [40], and Young (double-slit) [41] interferometers are based on gate-tuneable [42,43] spin precession [44] due to the Rashba effect [45] that arises from structural inversion asymmetry (SIA) [46] in semiconductor heterostructures. Spin-interference effects due to Rashba spin splitting are present in quantum networks [47] and multiple coherent scattering of electrons from intrinsic and artificial impurities [48].

Here we provide a review and more details of our recent studies of single [40] and two-particle [49] interference in spin-dependent Mach-Zehnder interferometers. The following Section is devoted to a brief introduction to SIA-induced (Rashba) spin splitting, discussing its salient features and relevance for spin-dependent interferometry. Single-particle interference effects and their possible use in spintronics and quantum information processing are discussed in Section 3. We provide results for two-particle interference and entanglement generation in Sec. 4. Our conclusions and an outlook to future work are presented in Sec. 5. A detailed analytical expression for the scattering matrix of the spin-dependent Mach-Zehnder interferometer discussed here is given in the Appendix.

2. Spin precession arising from SIA spin splitting

Two-dimensional (2D) electrons in asymmetric semiconductor heterostructures are subject to a coupling of their spin and orbital degrees of freedom [50] which gives rise to a correction

$$H_{\mathrm{R}} = \frac{\pi\hbar}{mL_{\mathrm{so}}} \; (\sigma_x p_y - \sigma_y p_x) \tag{2.1}$$

to their kinetic-energy term in the Hamiltonian. Here σ_x, σ_y denote Pauli matrices, p_x, p_y are the electron's in-plane momentum components, and the spin-precession length [44] L_{so} measures the strength of Rashba spin splitting [45] (and thus SIA of the heterostructure) in terms of a length scale. Typical values are $L_{\mathrm{so}} \sim 400$ nm in InGaAs/InP [43] and $\lesssim 100$ nm in HgTe/HgCdTe [51] heterostructures. Eigenstates of the 2D free-electron Hamitonian including the SIA spin-orbit term (2.1) are plane waves characterised by wave number $\vec{k} = (k_x, k_y)$. They are also eigenstates (with eigenvalue $\sigma = \pm 1$) of spin projection in the in-plane direction that is perpendicular to $\vec{k}$. The energy dispersion, given by

$$E_\sigma(\vec{k}) = \frac{\hbar^2}{2m} \left(k - \sigma \frac{\pi}{L_{\mathrm{so}}}\right)^2 - \frac{\pi^2 \hbar^2}{2mL_{\mathrm{so}}^2} \quad , \tag{2.2}$$

is spin-split but, unlike in the case of Zeeman splitting, SIA spin splitting does not result in a net magnetisation of the 2D system. At a fixed energy such as the Fermi energy, electron states are grouped into two circles in $\vec{k}$-space as shown in Fig. 1. For each propagation direction, two states
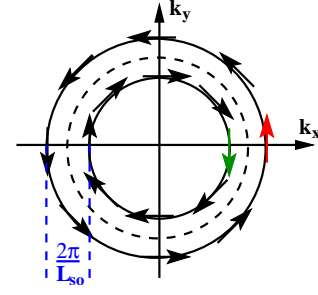

Fig. 1. Fermi surface of a 2D electron system with SIA spin splitting. For any propagation direction, two eigenstates exist with opposite spin and wave numbers differing by $2\pi/L_{\mathrm{so}}$. The spin quantisation axis for eigenstates is always perpendicular to their 2D wave vector and thus cannot be fixed globally for all eigenstates.

exist that have opposite spin polarisation perpendicular to $\vec{k}$ and wave vector differing by $2\pi/L_{\mathrm{so}}$.

There are two relevant consequences of SIA spin splitting for electron-wave interference in nanostructures. Firstly, the Fermi-wave-vector difference for opposite-spin states moving in the same direction results in different dynamical phases acquired by the corresponding two partial waves. As a result, a superposition of eigenstates injected in a wave guide will evolve during propagation to yield a precession of spin [52,53] with spatial period L_{so}. Gate-tuneability of SIA that gives rise to the spin splitting can be used to adjust [44] the spin-precession length and thus manipulate the spin state of electrons emerging from the wave guide. Secondly, the dependence of eigenstates' spin quantisation axis on the propagation direction implies that spin-conserving scattering of partial waves can induce spin precession of incident SIA-spin-split eigenstates. Figure 2 illustrates this fact for a beam splitter. No spin precession occurs for the electron state incident from the left and its transmitted partial wave emitted to the right because their spin is polarised perpendicular to the propagation direction. In contrast, the reflected partial wave has the same spin state as the incoming electron but moves in a direction that is perpendicular to the line of incidence. With spin and propa-
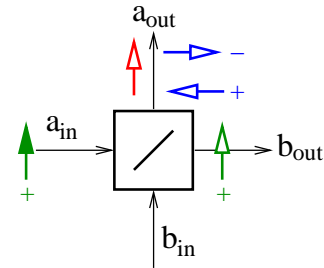

Fig. 2. Scattering of SIA-spin-split states at a beam splitter. The electron wave incoming from the left and its transmitted partial wave do not experience spin precession because they are in the spin-split eigenstate with $\sigma = +1$. This is not true for the reflected partial wave. As the latter's spin is parallel to its propagation direction, the reflected wave is a superposition of $\sigma = \pm 1$ eigenstates and its spin will precess. Within the scattering theory of quantum transport that we employ, the beam splitter is a four-terminal device characterised by a scattering matrix that relates quantum spinor amplitudes $a_{\mathrm{in}}, b_{\mathrm{in}}$ at the input terminals to those $(a_{\mathrm{out}}, b_{\mathrm{out}})$ at the output.
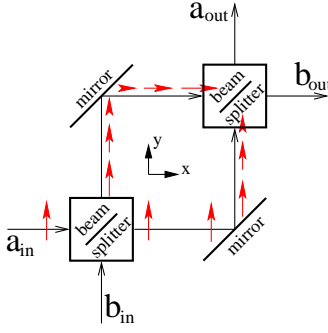
Fig. 3. Spin-dependent electronic Mach-Zehnder interferometer. Beam separation and spin precession for an electron wave incident from the left in an SIA-spin-split eigenstate are indicated. Our theoretical description of this device is based on its scattering matrix that can be obtained by suitable combination of the spin-resolved scattering matrices for its constituent parts.

gation direction now parallel for the reflected partial wave, it is a superposition of SIA eigenstates for this outgoing terminal and spin precession commences.

3. Spin-dependent Mach-Zehnder interferometer

The Mach-Zehnder (MZ) interferometer is routinely used in quantum optics [3]. Its basic structure, consisting of two beam splitters and two mirrors, is illustrated in Fig. 3. In the following, we consider electronic realisations of the interferometer, where quantum point contacts could be used for beam splitters [13–15] and mirror reflection occurs from etched walls. The presence of SIA spin splitting introduces spin precession of electron waves in the interferometer, as indicated in Fig. 3. Back-gate voltages could be used [42,43] to adjust the spin-precession length L_{so} *uniformly* in the interferometer structure. Note that, in contrast to other theoretical proposals [32,33,54,55], we do not employ local variations in the SIA spin splitting for our device concepts.

The function of each linear-optical device, as well as the acquisition of spin-dependent dynamical phases for travelling electron waves, can be described mathematically by appropriate scattering matrices [56] that relate outgoing and incoming quantum probability-wave amplitudes. We assume straight wave guides to be attached to each terminal of a beam splitter/mirror, making it possible to choose SIA-spin-split eigenstates as our scattering states. Using standard notation suitably generalised to our situation with spin-dependent scattering (see Ref. [40], especially Fig. 1 and Eq. (2), for our conventions), the $\mathcal{S}$-matrices for an ideal symmetric beam splitter, ideal mirror(s), and one-dimensional interferometer wave guides are, respectively,

$$\mathcal{S}_{bs} = \begin{pmatrix} \frac{i}{2} & -\frac{1}{2} & \frac{1}{\sqrt{2}} & 0 \\ -\frac{1}{2} & \frac{i}{2} & 0 & \frac{1}{\sqrt{2}} \\ \frac{1}{\sqrt{2}} & 0 & \frac{i}{2} & \frac{1}{2} \\ 0 & \frac{1}{\sqrt{2}} & \frac{1}{2} & \frac{i}{2} \end{pmatrix} \quad , \tag{3.1}$$

$$\mathcal{S}_{m} = \begin{pmatrix} \frac{i}{\sqrt{2}} & -\frac{1}{\sqrt{2}} & 0 & 0 \\ -\frac{1}{\sqrt{2}} & \frac{i}{\sqrt{2}} & 0 & 0 \\ 0 & 0 & \frac{i}{\sqrt{2}} & \frac{1}{\sqrt{2}} \\ 0 & 0 & \frac{1}{\sqrt{2}} & \frac{i}{\sqrt{2}} \end{pmatrix} \quad , \tag{3.2}$$

$$\mathcal{S}_{(x,y)} = \begin{pmatrix} 0 & 0 & e^{-\frac{i\pi y}{L_{so}}} & 0 \\ 0 & 0 & 0 & e^{\frac{i\pi y}{L_{so}}} \\ e^{-\frac{i\pi x}{L_{so}}} & 0 & 0 & 0 \\ 0 & e^{\frac{i\pi x}{L_{so}}} & 0 & 0 \end{pmatrix} \quad . \tag{3.3}$$

Due to the special MZ-interferometer design, the outputs from the first beam splitter become orthogonal mirror inputs. Essentially, each partial-wave beam can be considered to hit on a different side of a two-faced mirror before interfering with the other at the second beam splitter. We can therefore use $\mathcal{S}_m$ to simultaneously represent the effect of both mirrors. The scattering matrix of an entire MZ-interferometer structure is then obtained by simple multiplication of appropriate S-matrices:

$$\mathcal{S}_{MZ} = \mathcal{S}_{bs}\,\mathcal{S}_{sw}\,\mathcal{S}_{(w,h)}\,\mathcal{S}_{sw}\,\mathcal{S}_m\,\mathcal{S}_{sw}\,\mathcal{S}_{(w,h)}\,\mathcal{S}_{sw}\,\mathcal{S}_{bs}\,. \tag{3.4}$$

We omitted an unimportant phase factor $\exp\{ik_E(w+h)\}$ where k_E is the average of the two Fermi wave vectors for SIA-spin-split bands. The matrix $\mathcal{S}_{sw} = \sigma_x \otimes \sigma_x$ converts quantum amplitudes at the outgoing terminals of any interferometer part into incoming ones for the next. w and h are the spatial extensions of the MZ interferometer in x and y directions, respectively. The general analytic expression for $\mathcal{S}_{MZ}$ is given in the Appendix. Here we focus on a several special cases that are of potential interest to spintronics [23] and quantum information processing [57].

(i) w and h are integer multiples of the spin-precession length L_{so}. In this case, the MZ interferometer transmits any incoming state perfectly, except for a possible overall sign change of quantum amplitudes. This is the default situation [58] for a rectangularly shaped conventional Mach-Zehnder interferometer where the optical path lengths in the two interferometer arms are equal. Phase shifts due to reflections at beam splitters/mirrors then result in constructive (desctructive) interference in the transmitting (reflecting) channel. In the following, we demonstrate deviations from this canonical behaviour, which are entirely due to spin dependence of electron-wave interference.

(ii) w is an integer but h is a half-integer multiple of L_{so}. To be specific, let us assume $w = m\,L_{so}$ and $h = (n+1/2)L_{so}$. Then $\mathcal{S}_{MZ}$ reduces to

$$(-1)^{(m+n+\frac{1}{2})} \begin{pmatrix} 0 & 0 & 1 & 0 \\ 0 & 0 & 0 & -1 \\ 0 & i & 0 & 0 \\ -i & 0 & 0 & 0 \end{pmatrix} \quad .$$

3

The interferometer is still totally transmitting but, in the horizontal (x) direction, transmission of each SIA-split eigenstate is associated with a spin flip. Note that the interferometer's extension in this direction is an integer multiple of L_{so}; thus no spin flip could have been achieved for any spin state by transmission through a wave guide of the same length. More fundamentally, however, this spin flip occurs for SIA-split eigenstates (whose spin is polarised in the vertical direction). Such states would not precess and, hence, no spin flip could ever be engineered for these by transmission through a horizontal wave guide. On the other hand, the state with spin polarised in horizontal direction (i.e., parallel to the propagation direction) would be faithfully transmitted by this interferometer configuration. Obviously, an analogous situation where the behaviour of horizontal and vertical transmission of spin-split eigenstates is exchanged occurs when w is a half-integer and h an integer multiple of the spin-precession length.

(iii) Both w and h are half-integer multiples of L_{so}. The MZ-interferometer scattering matrix for this case can be written, upto an overall sign, as $\mathcal{S}_m^*$, i.e., it is the complex conjugate of the mirror's S-matrix. Evidently, the interferometer is now purely reflecting, which constitutes a drastic departure from the canonical behaviour of a MZ interferometer [58]. Interestingly, cases (i) and (iii) can be realised for any quadratic interferometer (i.e., having $w = h$) by suitable adjustment of L_{so}. This enables the design of a magnet-less spin-controlled field-effect transistor [40,41].

(iv) w is an integer multiple and h a quarter-integer multiple of L_{so}. Upto an overall sign, the MZ interferometer's S-matrix for this case can be written as

$$\begin{pmatrix} 0 & 0 & (-1)^{-1/4} & 0 \\ 0 & 0 & 0 & (-1)^{1/4} \\ \dfrac{1}{\sqrt{2}} & \dfrac{1}{\sqrt{2}} & 0 & 0 \\ -\dfrac{1}{\sqrt{2}} & \dfrac{1}{\sqrt{2}} & 0 & 0 \end{pmatrix}.$$

Thus the interferometer is fully transmitting and realises a (pseudo-)Hadamard transformation [57] in the horizontal channel. An analogous configuration with a Hadamard transformation for the vertical channel can be obtained by having w instead of h be a quarter-integer multiple of L_{so}.

(v) Any serial combination of two (or more) MZ interferometers can be discussed as well. Geometric considerations suggest that additional mirrors would have to be inserted, and spin-dependent phase shifts be accounted for. We choose to neglect the latter (possible in the limit when the path length between the two interferometers is much smaller than the spin-precession length) but include the mirrors. As an example, we give results for an interferometer of type (iv) in series with one of type (iii). Again neglecting a possible overall sign change of quantum amplitudes, the scattering matrix for the two-interferometer setup is

$$i \begin{pmatrix} 0 & 0 & 0 & (-1)^{3/4} \\ 0 & 0 & (-1)^{-3/4} & 0 \\ \dfrac{1}{\sqrt{2}} & \dfrac{1}{\sqrt{2}} & 0 & 0 \\ \dfrac{1}{\sqrt{2}} & -\dfrac{1}{\sqrt{2}} & 0 & 0 \end{pmatrix}.$$

Here the horizontally transmitting channel is subject to a Hadamard transformation. Scattering states in the vertical channel experience a spin flip. In contrast, spin eigenstates for projection parallel to the propagation direction in the vertical channel are eigenstates of the transmission matrix.

For the present discussion, it shall suffice to present the above examples. Inspection of the general scattering matrix for spin-dependent MZ interferometers, which is given in the Appendix, can be used to design yet more devices.

4. Spin-dependent two-particle interference and entanglement generation

In the previous Section, we discussed phenomena arising from electron probability waves interfering with themselves in a MZ-interferometer setup. The question immediately arises whether the interplay between spin-dependent interference and Fermi statistics can give rise to nontrivial two-particle effects. After all, it is well-known that the Pauli principle affects multi-particle scattering events, e.g., at a beam splitter [59]. We investigated this question by means of a two-particle scattering approach. Its basic ingredient is the definition of a suitable basis of two-particle scattering states. The quantum numbers to use for distinguishing single-particle states are the interferometer terminal (a or b) and the SIA-spin-split subband quantum number ($\sigma = \pm 1$). Thus the single-particle Hilbert space is four-dimensional. A straightforward consideration yields that the corresponding two-particle Hilbert space for fermionic particles is six-dimensional. We found it useful to employ a basis of Bell states similar to the one introduced in Ref. [60],

$$|\chi_1\rangle = \frac{1}{\sqrt{2}} \left(c_{a+}^\dagger c_{a-}^\dagger + c_{b+}^\dagger c_{b-}^\dagger \right) |0\rangle \quad , \tag{4.1}$$

$$|\chi_2\rangle = \frac{1}{\sqrt{2}} \left(c_{a+}^\dagger c_{b+}^\dagger - c_{a-}^\dagger c_{b-}^\dagger \right) |0\rangle \quad , \tag{4.2}$$

$$|\chi_3\rangle = \frac{1}{\sqrt{2}} \left(c_{a+}^\dagger c_{b-}^\dagger + c_{a-}^\dagger c_{b+}^\dagger \right) |0\rangle \quad , \tag{4.3}$$

$$|\chi_4\rangle = \frac{i}{\sqrt{2}} \left(c_{a+}^\dagger c_{a-}^\dagger - c_{b+}^\dagger c_{b-}^\dagger \right) |0\rangle \quad , \tag{4.4}$$

$$|\chi_5\rangle = \frac{i}{\sqrt{2}} \left(c_{a+}^\dagger c_{b+}^\dagger + c_{a-}^\dagger c_{b-}^\dagger \right) |0\rangle \quad , \tag{4.5}$$

$$|\chi_6\rangle = \frac{i}{\sqrt{2}} \left(c_{a+}^\dagger c_{b-}^\dagger - c_{a-}^\dagger c_{b+}^\dagger \right) |0\rangle \quad , \tag{4.6}$$

where the operator $c_{\alpha\sigma}^\dagger$ creates an electron at the Fermi energy in the interferometer arm α and with SIA spin-split subband quantum number σ. Any two–electron state $|i\rangle$ ($|o\rangle$) at the input (output) can be expressed as a linear

combination of these basis states. Using our previous results for spin-resolved single-particle scattering matrices at beam splitters, mirrors, etc. and straightforwardly implementing the Pauli principle, we derived [49] the 6×6 scattering matrices that can be used to calculate the two-particle state generated at the output of a linear-optical device from any incoming state that is expressed as a linear superposition of the $|\chi_j\rangle$. Suitable combination of the individual devices' two-particle scattering matrices, in a way that is similar to the single-particle case, yields the corresponding two-particle scattering matrix for the entire interferometer. Its complicated analytical expression is omitted here.

Again, a variety of special cases can be considered that are distinguished by different shapes/sizes of the interferometer, as well as different two-particle input configurations. In the following, we focus on the situation where a two-particle product state with double-occupancy is incident in one interferometer arm, while the other input terminal is kept floating. See Figure 4 for an illustration. To be specific, we consider the state $|i_{dbl}\rangle = c_{a+}^\dagger c_{a-}^\dagger |0\rangle$. The output state generated from it by the MZ interferometer will be a superposition of states having single electron occupancy in each output arm with others that have a finite amplitude for double occupancy in one of them. Let us assume that we have installed a device to measure the electron number (i.e., charge) in one of the output terminals [21]. Performing this measurement each time we send in two electrons with opposite spin at the input channel, we will obtain values 0, 1, or 2 with certain frequencies. The charge measurement leaves the spin and orbital wave functions of output states unaffected, but it allows us to filter out those states where exactly one electron is scattered into each of the output arms. Calculation of the concurrence [61] proves that, by preparing the input state $c_{a+}^\dagger c_{a-}^\dagger |0\rangle$ and choosing states at the interferometer output for which exactly one electron lives in each output arm, we obtain two-electron states that are maximally entangled in the SIA-spin-split subband quantum number σ and the output-terminal index (a and
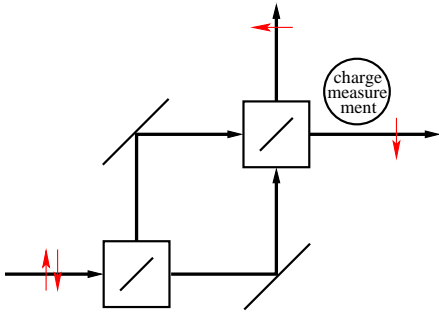

Fig. 4. Two-particle scattering and entanglement generation at the spin-dependent Mach-Zehnder interferometer. A non-entangled input state incident from the left is transformed into an output state that has a finite probability for single-particle occupancy in each output arm. A charge measurement at the device's output enables us to select such cases non-deterministically. It turns out that the corresponding output states are always maximally entangled in the SIA-spin-split subband quantum number.
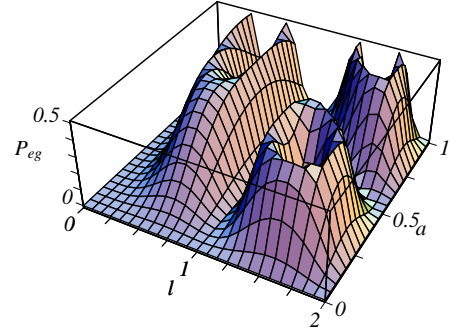

Fig. 5. Efficiency P_{eg} of entanglement generation by the procedure illustrated in Fig. 4, calculated for rectangular MZ interferometers of width lL_{so} and aspect ratio a.

b). The efficiency P_{eg} for this nondeterministic scheme of entanglement generation is given by the probability of producing the output state with single-electron occupancy per output arm from the input state $|i_{dbl}\rangle$. This quantity turns out to depend on the interferometer size and geometry. As in the previous Section, we consider a rectangular MZ interferometer of width w and height h. Figure 5 shows a plot of P_{eg} for a certain range of dimensionless parameters $l = w/L_{so}$ and $a = h/w$. The largest possible value of P_{eg} is 50%, i.e., the same as the efficiency of entanglement generation at a single beam splitter [62]. Unlike such a beam splitter, however, the MZ interferometer can be tuned by an external gate voltage, which controls the parameter l by adjusting L_{so} [42,43], between maximum and zero entanglement generation. This realises a switcheable entangler.

5. Conclusions and outlook

We presented theoretical results for spin-dependent single and two-particle interference in an electronic Mach-Zehnder interferometer with a uniform electric-field-tuneable spin splitting. Analytic expressions are obtained for scattering matrices, enabling us to study realisations of spintronic devices and quantum gates. With single electrons as input, spin-dependent interference enables the design of a magnet-less spin-controlled field-effect switch. Single-qubit gates such as the Hadamard gate can also be realised. Introduction of an additional charge measurement at the interferometer output makes it possible to generate entangled mobile-electron spins nondeterministically. The efficiency of entanglement generation can be tuned between 0 and 50% by adjusting the spin-precession length using external gate voltages. Future work will be focused on applying methods presented here to study other promising spin-dependent interference devices, e.g., modeled after the Michelson and Franson [63] interferometers.

Acknowledgements

Appendix A. Analytical expression for the general MZ-interferometer scattering matrix

$$
\mathcal{S}_{\mathrm{MZ}} =
\begin{pmatrix}
-\dfrac{i\sin\left(\frac{\pi h}{L_{\mathrm{so}}}\right)\sin\left(\frac{\pi w}{L_{\mathrm{so}}}\right)}{\sqrt{2}} & -\dfrac{\sin\left(\frac{\pi h}{L_{\mathrm{so}}}\right)\sin\left(\frac{\pi w}{L_{\mathrm{so}}}\right)}{\sqrt{2}} & -e^{-\frac{i\pi h}{L_{\mathrm{so}}}}\cos\left(\frac{\pi w}{L_{\mathrm{so}}}\right) & \cos\left(\frac{\pi h}{L_{\mathrm{so}}}\right)\sin\left(\frac{\pi w}{L_{\mathrm{so}}}\right) \\[3ex]
-\dfrac{\sin\left(\frac{\pi h}{L_{\mathrm{so}}}\right)\sin\left(\frac{\pi w}{L_{\mathrm{so}}}\right)}{\sqrt{2}} & -\dfrac{i\sin\left(\frac{\pi h}{L_{\mathrm{so}}}\right)\sin\left(\frac{\pi w}{L_{\mathrm{so}}}\right)}{\sqrt{2}} & -\cos\left(\frac{\pi h}{L_{\mathrm{so}}}\right)\sin\left(\frac{\pi w}{L_{\mathrm{so}}}\right) & -e^{\frac{i\pi h}{L_{\mathrm{so}}}}\cos\left(\frac{\pi w}{L_{\mathrm{so}}}\right) \\[3ex]
-e^{-\frac{i\pi w}{L_{\mathrm{so}}}}\cos\left(\frac{\pi h}{L_{\mathrm{so}}}\right) & -\cos\left(\frac{\pi w}{L_{\mathrm{so}}}\right)\sin\left(\frac{\pi h}{L_{\mathrm{so}}}\right) & -\dfrac{i\sin\left(\frac{\pi h}{L_{\mathrm{so}}}\right)\sin\left(\frac{\pi w}{L_{\mathrm{so}}}\right)}{\sqrt{2}} & \dfrac{\sin\left(\frac{\pi h}{L_{\mathrm{so}}}\right)\sin\left(\frac{\pi w}{L_{\mathrm{so}}}\right)}{\sqrt{2}} \\[3ex]
\cos\left(\frac{\pi w}{L_{\mathrm{so}}}\right)\sin\left(\frac{\pi h}{L_{\mathrm{so}}}\right) & -e^{\frac{i\pi w}{L_{\mathrm{so}}}}\cos\left(\frac{\pi h}{L_{\mathrm{so}}}\right) & \dfrac{\sin\left(\frac{\pi h}{L_{\mathrm{so}}}\right)\sin\left(\frac{\pi w}{L_{\mathrm{so}}}\right)}{\sqrt{2}} & -\dfrac{i\sin\left(\frac{\pi h}{L_{\mathrm{so}}}\right)\sin\left(\frac{\pi w}{L_{\mathrm{so}}}\right)}{\sqrt{2}}
\end{pmatrix}
\tag{A.1}
$$

References

[1] P. Rogers, Phys. World 15 (9) (2002) 15.
[2] A. Tonomura, J. Endo, T. Matsuda, T. Kawasaki, H. Ezawa, Am. J. Phys. 57 (1989) 117.
[3] R. Loudon, The Quantum Theory of Light, 3rd Edition, Oxford University Press, Oxford, UK, 2000.
[4] L. L. Sohn, L. P. Kouwenhoven, G. Schön (Eds.), Mesoscopic Electron Transport, Vol. 345 of NATO ASI Series E, Kluwer Academic, Dordrecht, The Netherlands, 1997.
[5] Y. Imry, Introduction To Mesoscopic Physics, 2nd Edition, Oxford University Press, New York, 2002.
[6] Y. Aharonov, D. Bohm, Phys. Rev. 115 (1959) 485.
[7] R. A. Webb, S. Washburn, C. P. Umbach, R. B. Laibowitz, Phys. Rev. Lett. 54 (1985) 2696.
[8] G. Timp, A. M. Chang, J. E. Cunningham, T. Y. Chang, P. Mankiewich, R. Behringer, R. E. Howard, Phys. Rev. Lett. 58 (1987) 2824.
[9] B. J. van Wees, L. P. Kouwenhoven, C. J. P. M. Harmans, J. G. Williamson, C. E. Timmering, M. E. I. Broekaart, C. T. Foxon, J. J. Harris, Phys. Rev. Lett. 62 (1989) 2523.
[10] P. G. N. de Vegvar, G. Timp, P. M. Mankiewich, R. Behringer, J. Cunningham, Phys. Rev. B 40 (1989) 3491–3494.
[11] W. G. van der Wiel, Y. V. Nazarov, S. De Franceschi, T. Fujisawa, J. M. Elzermann, E. W. G. M. Huizeling, S. Tarucha, L. P. Kouwenhoven, Phys. Rev. B 67 (2003) 033307.
[12] A. Yacoby, M. Heiblum, V. Umansky, H. Strikman, D. Mahalu, Phys. Rev. Lett. 73 (1994) 3149.
[13] M. Henny, S. Oberholzer, C. Strunk, T. Heinzel, K. Ensslin, M. Holland, C. Schönenberger, Science 284 (1999) 296.
[14] W. D. Oliver, J. Kim, R. C. Liu, Y. Yamamoto, Science 284 (1999) 299.
[15] Y. Ji, Y. Chung, D. Sprinzak, M. Heiblum, D. Mahalu, H. Strikman, Nature (London) 422 (2003) 415.
[16] I. Neder, M. Heiblum, Y. Levinson, D. Mahalu, V. Umansky, Phys. Rev. Lett. 96 (2006) 016804.
[17] M. A. Topinka, B. J. LeRoy, R. M. Westervelt, S. E. J. Shaw, R. Fleischmann, E. J. Heller, K. D. Maranowski, A. C. Gossard, Nature (London) 410 (2001) 183.
[18] B. J. LeRoy, A. C. Bleszynski, K. E. Aidala, R. M. Westervelt, E. J. Heller, S. E. J. Shaw, K. D. Maranowski, A. C. Gossard, Phys. Rev. Lett. 94 (2005) 1268012.
[19] S. Datta, Quantum Transport: Atom to Transistor, Cambridge University Press, Cambridge, UK, 2005.
[20] E. Knill, R. Laflamme, G. J. Milburn, Nature 409 (2001) 46.
[21] C. W. J. Beenakker, D. P. DiVincenzo, C. Emary, M. Kindermann, Phys. Rev. Lett. 93 (2004) 020501.
[22] S. A. Wolf, D. D. Awschalom, R. A. Buhrmann, J. M. Daughton, S. von Molnár, M. L. Roukes, A. Y. Chtchelkanova, D. M. Treger, Science 294 (2001) 1488.
[23] D. D. Awschalom, D. Loss, N. Samarth (Eds.), Semiconductor Spintronics and Quantum Computation, Springer Verlag, Berlin, 2002.
[24] I. Zutić, J. Fabian, S. Das Sarma, Rev. Mod. Phys. 76 (2004) 323.
[25] S. Egger, C. H. Back, J. Krewer, D. Pescia, Phys. Rev. Lett. 83 (1999) 2833.
[26] S. Egger, C. H. Back, D. Pescia, J. Appl. Phys. 87 (2000) 7142.
[27] J. B. Yau, E. P. De Poortere, M. Shayegan, Phys. Rev. Lett. 88 (2002) 146801.
[28] Y. K. Kato, R. C. Myers, A. C. Gossard, D. D. Awschalom, Appl. Phys. Lett. 86 (2005) 162107.
[29] M. König, A. Tschetschetkin, E. M. Hankiewicz, J. Sinova, V. Hock, V. Daumer, M. Schäfer, C. R. Becker, H. Buhmann, L. W. Molenkamp, Phys. Rev. Lett. 96 (2006) 076804.
[30] T. Koga, Y. Sekine, J. Nitta, Phys. Rev. B 74 (2006) 041302(R).
[31] J. Nitta, F. E. Meijer, H. Takayanagi, Appl. Phys. Lett. 75 (1999) 695.
[32] R. Ionicioiu, I. D'Amico, Phys. Rev. B 67 (2003) 041307(R).
[33] A. A. Kiselev, K. W. Kim, J. Appl. Phys. 94 (2003) 4001.
[34] B. Molnár, F. M. Peeters, P. Vasilopoulos, Phys. Rev. B 69 (2004) 155335.
[35] D. Frustaglia, K. Richter, Phys. Rev. B 69 (2004) 235310.
[36] S. Souma, B. K. Nikolic, Phys. Rev. B 70 (2004) 195346.
[37] P. Földi, O. Kálmán, M. G. Benedict, F. M. Peeters, Phys. Rev. B 73 (2006) 155325.
[38] A related two-terminal Rashba-interferometer setup was recently proposed by M.-H. Liu, K.-W. Chen, S.-H. Chen, and C.-R. Chang, cond-mat/0611077.
[39] T. Koga, J. Nitta, M. van Veenhuizen, Phys. Rev. B 70 (2004) 161302(R).
[40] U. Zülicke, Appl. Phys. Lett. 85 (2004) 2616.
[41] U. Zülicke, J. Supercond.: Incorp. Novel Magn. 18 (2005) 241.

[42] J. Nitta, T. Akazaki, H. Takayanagi, T. Enoki, Phys. Rev. Lett. 78 (1997) 1335.

[43] G. Engels, J. Lange, T. Schäpers, H. Lüth, Phys. Rev. B 55 (1997) R1958.

[44] S. Datta, B. Das, Appl. Phys. Lett. 56 (1990) 665.

[45] Y. A. Bychkov, E. I. Rashba, J. Phys. C 17 (1984) 6039.

[46] R. Winkler, Phys. Rev. B 62 (2000) 4245.

[47] D. Bercioux, M. Governale, V. Cataudella, V. Marigliano Ramaglia, Phys. Rev. Lett. 93 (2004) 056802.

[48] J. D. Walls, J. Huang, R. M. Westervelt, E. J. Heller, Phys. Rev. B 73 (2006) 035325.

[49] A. I. Signal, U. Zülicke, Appl. Phys. Lett. 87 (2005) 102102.

[50] R. Winkler, Spin-Orbit Coupling Effects in Two-Dimensional Electron and Hole Systems, Vol. 191 of Springer Tracts in Modern Physics, Springer, Berlin, 2003.

[51] Y. S. Gui, C. R. Becker, N. Dai, J. Liu, Z. J. Qiu, E. G. Novik, M. Schäfer, X. Z. Shu, J. H. Chu, H. Buhmann, L. W. Molenkamp, Phys. Rev. B 70 (2004) 115328.

[52] S. A. Crooker, D. L. Smith, Phys. Rev. Lett. 94 (2005) 236601.

[53] Y. K. Kato, R. C. Myers, A. C. Gossard, D. D. Awschalom, Appl. Phys. Lett. 87 (2005) 022503.

[54] J. C. Egues, G. Burkard, D. Loss, Phys. Rev. Lett. 89 (2002) 176401.

[55] A. Sarkar, T. K. Bhattacharyya, A. Patwardhan, Appl. Phys. Lett. 88 (2006) 213113.

[56] G. Feve, W. D. Oliver, M. Aranzana, Y. Yamamoto, Phys. Rev. B 66 (2002) 155328.

[57] M. A. Nielsen, I. L. Chuang, Quantum Computation and Quantum Information, Cambridge University Press, Cambridge, UK, 2000.

[58] K. P. Zetje, S. F. Adams, R. M. Tocknell, Phys. Educ. 35 (2000) 46.

[59] R. Loudon, Phys. Rev. A 58 (1998) 4904.

[60] K. Eckert, J. Schliemann, D. Bruß, M. Lewenstein, Ann. Phys. (NY) 299 (2002) 88.

[61] W. K. Wootters, Phys. Rev. Lett. 80 (1998) 2245.

[62] S. Bose, D. Home, Phys. Rev. Lett. 88 (2002) 050401.

[63] J. D. Franson, Phys. Rev. Lett. 62 (1989) 2205.